Biol. Cybern. 69, 463–473 (1993)

Biological Cybernetics
© Springer-Verlag 1993

Dynamic properties of cortical evoked (10 Hz) oscillations: theory and experiment

Klaus Kopecz, Gregor Schöner, Friederike Spengler, Hubert R. Dinse

Institut für Neuroinformatik-ND 04, Universität Bochum, Universitätsstrasse, D-44780 Bochum, Germany

Received: 23 January 1993/Accepted in revised form: 24 May 1993

Abstract. Experiments probed the dynamic properties of stimulus-evoked (≈ 10 Hz) oscillations in somatosensory cortex of anesthetized rats. Experimental paradigms and statistical time series analysis were based on theoretical ideas from a dynamic approach to temporal patterns of neuronal activity. From the results of a double-stimulus paradigm we conclude that the neuronal response contains two components with different dynamics and different coupling to the stimulus. Based on this result a quantitative dynamic model is derived, making use of normal form theory for bifurcating vector fields. The variables used are abstract, but measurable, dynamic components. The model parameters capture the dynamic properties of neuronal response and are related to experimental results. A structural interpretation of the model can be given in terms of the collective dynamics of neuronal groups, their mutual interaction, and their coupling to peripheral stimuli. The model predicts the stimulus-dependent lifetime of the oscillations as observed in experiment. We show that this prediction relies on the basic concept of dynamic bistability and does not depend on the modeling details.

1 Introduction

Stimulus-evoked oscillatory responses in the alpha range in primary cortical and thalamic structures have been studied for a long time (e.g., Bishop and O'Leary 1936; Andersen and Andersson 1968) on the EEG [see Basar (1980) for a review; Basar et al. 1992) and the single-cell level [see Steriade et al. (1990) for a review]. The functional role of these rhythms has remained elusive. Hypotheses include "gating" of sensory input (Llinás and Sasaki 1989) and contributions to temporal properties of receptive fields (Dinse et al. 1990). An important question for such functional interpretations is how the oscillatory response depends on the temporal structure of the stimulation. In the earlier studies such dependence has been looked at mainly in terms of effects on response amplitude. For instance, Aitkin et al. (1966) showed that the amplitude of the oscillatory response is modulated as the interval between two subsequent stimuli is varied. Similar results were obtained by Adrian (1941) and Chang (1950).

In this study we address in detail the question of how the temporal structure of the oscillatory response depends on the temporal structure of the stimulation. We refer to experimental data reported in part in Schöner et al. (1992). Evoked (≈ 10 Hz) oscillations were observed in single-cell (extracellular) recordings from the hindpaw representation in area SI in the somatosensory cortex of anesthetized rats. Stimulation consisted of computer-controlled taps within the receptive fields. A two-stimulus paradigm was used in which a first stimulus started the oscillation and a second stimulus was placed at specific phases of the ongoing oscillation. Earlier empirical studies (Chang 1950; Andersen and Andersson 1968; Llinás and Sasaki 1989) reported qualitatively that an oscillatory response started by a conditioning stimulus can be "reset" by a subsequent test stimulus.

We found (1) that the complete phase resetting curve is continuous, indicating that the coupling between oscillatory response and the stimulus is phase dependent and (2) that two response components must be distinguished, only one of which can be reset in the sense reported earlier. The transfer component (TC), visible as a short latency response immediately after a peripheral tap, is strictly stimulus locked and can be evoked any time. The oscillatory component (OC), visible as 2–7 peaks in the poststimulus-time histogram (PSTH) [or in averaged or unaveraged local field potential (LFP) recordings] is stimulus locked only when elicited from the resting state. But once started the detailed timing of the OC with respect to a second stimulus within the ongoing response depends on the current phase of oscillation and varies between the two extremes "resetting" and "going through".

In this article we present a theoretical approach to temporal structure in neuronal response that is based on the ideas of collective variables and nonlinear dynamics. The theoretical strategy is used to construct an exemplary model for stimulus-evoked oscillations. We derive the dynamic properties of temporal patterns in this

Correspondence to: K. Kopecz

model and perform further analysis on the experimental data of Schöner et al. (1992) to verify these predictions.

The theoretical ideas differ somewhat from the typical neuronal modeling approach, but are related to work in neuronal and behavioral patterns of coordinated movement [for review, see Schöner and Kelso (1988)]. Three assumptions form the basis of the theoretical strategy: (1) the temporal structure of neuronal response is reflective of the activity of neuronal groups and can be characterized by effective or collective variables; (2) the generation of this time structure can be understood as resulting from dynamic laws which represent the collective properties of the neuronal groups and which can be modeled as equations of motion of the collective variables; (3) stimuli act on these dynamics as time-dependent forces. The dynamic variables are related to the experimentally observable neuronal response in terms of measures of temporal structure such as peak latencies, interpeak intervals, and peak amplitudes (see below). Their dynamics are constrained by mapping observed stationary and self-generated time structure onto attractor solutions. To determine an actual functional form of a concrete dynamical model the definition of attractors and their stability as a function of experimental parameters must be supplemented by additional, more technical, assumptions (e.g., smoothness of the vector field and symmetries). Despite the phenomenological spirit of this strategy, we are able to show that such abstract dynamic models possess predictive power. A strong point is that model parameters relate directly to observed patterns. Moreover, the approach generates experimental paradigms and methods of analysis.

In Sect. 2 the experimental methods, extracted measures, and main experimental results are reported. In Sect. 3 a dynamic model is constructed and analyzed, and its parameters are related to experiment. A testable prediction is derived from the basic concept of dynamic bistability and is compared with the experimental data. The relation of the theoretical approach developed here to reductionistic neuronal modeling is clarified.

2 Experiments

2.1 Methods

Details on animal preparation and recording techniques were reported in Schöner et al. (1992). Rats were anesthetized (Nembutal in 2 rats, Urethan in 31 rats) and placed in a stereotactic apparatus. Recordings were made from the SI area with glass microelectrodes (1–2 MΩ) filled with concentrated NaCl. Both single unit and multi unit activity was stored on a personal computer. Field potentials were obtained simultaneously from the same electrode.

2.2 Data analysis

Neurophysiologists have used double-stimulus paradigms for decades, although often motivated by other concerns (e.g., Movshon et al. 1978; Ganz and Felder 1984). In the context of oscillatory response components the paradigm has been used repeatedly (Aitkin et al. 1966; Andersen and Andersson 1968; Llinás and Sasaki 1989), although the temporal structure of the oscillatory response has not been systematically and/or quantitatively analyzed in these cases. Such analysis is done here on the basis either of post-stimulus-time-histograms (PSTHs) obtained from single and multi unit activity or of averaged, and in some cases individual, local field-potential records. In both cases, the analysis proceeds in interactive computer displays in which peaks of activity can be recognized visually or based on algorithms (see Fig. 1 for illustration). The parameters – time of occurrence of a peak T_i and response amplitude at the peak A_i – are determined for each peak. In the case of PSTH-based analysis, the mass of the peak M_i (number of action potentials in a peak which is delimited by minima of activity) could likewise be extracted. The peaks are numbered beginning from the last stimulus applied, with the peaks following the conditioning stimulus referred to by the unprimed letters, T_i, A_i, and M_i, and the peaks following the test stimulus referred to by primed letters, T'_i, A'_i, and M'_i. From the peak measures we derive cycle times $Z_i = T_{i+1} - T_i$ (correspondingly for the primed measures). We call T_0 the latency of the response. To quantify the relative width of a peak, we consider the ratio of peak mass to peak amplitude, $W_i = M_i/A_i$.

For a given cell, we varied the interstimulus inverval (ISI) between conditioning and test stimulus from 40 to 350 ms in steps of 10 ms, and up to 1000 ms in 100 ms steps. This led to 39 conditions per cell (that means, we recorded 39 PSTHs per cell, each PSTH derived from 32 repetitions). To obtain estimates of the properties of the oscillations evoked by a single stimulus we pooled all measures derived for the first four peaks in the response to the conditioning stimulus as long as they occurred before the second tap. We call the resulting ensemble the

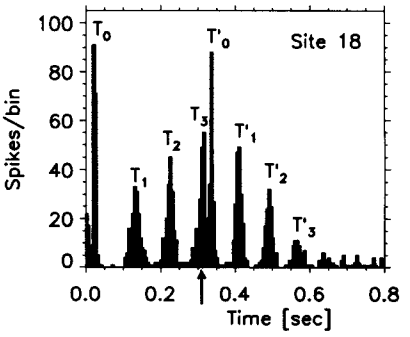

Fig. 1. Summed post-stimulus-time histogram (PSTH) derived from the double-stimulus paradigm from unit 18 with 32 repetitions. Binsize equals 5 ms. The labeling of peaks is indicated in terms of peak times (time of maximal spike rate). In addition, we extracted peak amplitudes (maximal spike rate for each peak) and peak masses (area under a peak). The time of the second stimulation is indicated by the arrow at 310 ms. Note that the first cycle time $Z_1 = T_1 - T_0$ equals 109 ms, whereas the cycle time $Z'_1 = T'_1 - T'_0$ equals 74 ms. The difference $T'_1 - T_3$ equals 92 ms, which is identical to the cycle times Z_2 and Z_3. This is an example where the oscillatory response "goes through" the second stimulation

oscillations per se (OPS). The second ensemble was built from the primed measures derived from the responses to the test stimulus. This was used to study effects of ISI on the response measures reflecting state dependence of the stimulus coupling.

2.3 Results

Of a total of 48 cells recorded, 25 cells were selected for detailed quantitative analysis on the basis of having a complete ISI scan. The temporal characteristics are reported from the PSTH analysis only, because all temporal effects have been reproduced with LFP recordings.

The analysis of the quantitative measures of response time structure, T_i, Z_i, A_i, and M_i, for the OPS ensemble revealed that the first peak of the response, which appears on the average at latency $T_0 = 21.7$ ms ($\pm$ 0.8 in repetitions of PSTH for the same cell/$\pm$ 2.1 across cells), differs from the subsequent peaks:

1. The first cycle time is larger than subsequent ones (significant[1] for 91% of cells), whereas in most cells we found no significant difference among the subsequent cycles ($Z_2 \neq Z_3$, for 9%). On the average we found $Z_1 = 119.9$ ms ($\pm$ 5.4/17.6), $Z_2 = 96.6$ ms ($\pm$ 7.2/12.0), $Z_3 = 84.4$ ms ($\pm$ 11.2/11.4).
2. The first peak is less variable in timing than the following peaks [$SD(T_{1,2,3}) > SD(T_0)$, for 100%].
3. The shape of the first peak differs from the subsequent peaks, being much sharper ($W_{1,2,3} > W_0$, for 100%, with $W_1 \approx W_2 \approx W_3 \approx 5W_0$).
4. Obviously, the first peak has much higher amplitude for all cells. Importantly, the amplitudes of the subsequent peaks do not differ from each other significantly. This means, in particular, that the oscillation does not have the appearance of a damped transient oscillation.
5. The initial response peak can be elicited reliably every time by stimulation, whereas the following peaks occur probabilistically in variable numbers. These peaks have a probability of not occurring at all. Further support for the distinction between the initial response peak and the subsequent oscillatory peaks is provided by the analysis of the effects of repeated stimulation (see below).

To select cells for the detailed analysis of the effect of ISI on the temporal structure of the response to the test stimulus, we employed the restrictive criterion that for at least one ISI condition the PSTH shows a discernible fourth peak preceding the test stimulus (there were roughly 11 possible ISI conditions where a fourth OPS peak would fit into the interval before the test stimulus). Eleven cells of 25 (or 44%) were oscillatory in this sense. These cells were now analyzed with respect to the influence of the test stimulus on the response characteristics by comparing primed measures with OPS measures. We found $Z'_1 < Z_1$ (significant for 82% of oscillating cells), $Z'_2 < Z_2$ (55%), and no significant difference between Z'_3 and Z_3. This indicates that the oscillation after the test stimulus is not simply a restarted version of the response to the conditioning stimulus, because in that latter case we would expect Z'_1 to be equal to Z_1.

To examine the functional dependence on ISI of the timing of oscillatory peaks after the test stimulus we plotted peak times as a function of ISI. The effects are salient for cells with very pronounced oscillations. The oscillatory peaks tend to lie close to those points in time where they would be expected if the oscillation started by the conditioning stimulus had "gone through" (cf. Fig. 1 and Fig. 5C). In cells with less pronounced oscillations this effect is not as salient. Statistical tests of Z'_1 showed, however, that this quantity is significantly more variable than the corresponding Z_1, indicating an effect of ISI. (The corresponding F test is equivalent to a one-factor analysis of variance testing for the effect of ISI.)

3 Dynamic theory

3.1 Modeling the two dynamic components

Following the theoretical strategy outlined in Sect. 2 we introduce variables to capture the observed response behavior. Graded and signed variables are assigned separately to the two response components with different dynamical properties. While it is not intended to model detailed response time curves (because these are not reproducible), the variables may best be compared with local field potentials.

The TC, modeling the short latency response, must span an at least two-dimensional phase space in order to account for the observed nonzero latencies. Restricting the modeling to the minimal two dimensions u_1, u_2, we assume that by choice of coordinates the observed component is u_1. For mathematical convenience we combine the two real variables into a single complex variable $u := u_1 + iu_2$. The transient response is described as relaxation to a single fixed point of, in leading order, a linear dynamics:

$$\dot{u} = c_u u$$

$$c_u := \alpha_u + i\omega_u \tag{1}$$

ω_u represents the eigenfrequency and α_u the negative damping of the TC. For stability we require $\alpha_u < 0$. The stimulus is described in leading order by a time-dependent, additive force:

$$\dot{u} = c_u u + FS(t)$$

$$F := F_1 + iF_2 \tag{2}$$

A single stimulus event (a tap to the hindpaw) is represented as a delta pulse, $\delta(t - t_0)$, where t_0 is the time of stimulation. A series $S(t)$ of stimulation events at times $t_i, i = 0, 1, \ldots$, with identical strength is represented by the sum

$$S(t) := \sum_i \delta(t - t_i) \tag{3}$$

[1] To compare mean values and variabilities we employed here and below, standard T- and F-test procedures. All stated results refer to a significance level of 1%

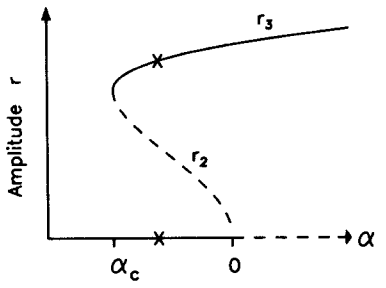

Fig. 2. Bifurcation diagram for the variation of a parameter α measuring the strength of stimulation. *Continuous lines* correspond to amplitudes of stable, oscillatory solutions and *dashed lines* to unstable ones. As α crosses some critical value α_c, a pair of oscillatory solutions with amplitudes r_2 and r_3 appear (global bifurcation), one stable, the other unstable. As α is increased further, the zero amplitude solution $r = 0$ (fixed point) loses stability at $\alpha = 0$, and only the oscillatory state remains stable. In the open interval $]\alpha_c, 0[$ two stable states coexist, as indicated by two *crosses* for some intermediate value of α. In this region the system switches spontaneously between these two states by noise-induced transitions

In the double-stimulus paradigm we have $S(t) = \delta(t) + \delta(t - I)$, where I is the variable ISI. The complex coupling strength F is used in polar coordinates:

$$F = |F| \exp(i\Phi_F) \tag{4}$$

For stimulation from the resting state $u(t = 0) = 0$, the relation of the parameters introduced so far to the experimental measures latency-peak time T_0 and latency-peak amplitude A_0 is:

$$\Phi_F = -\omega_u T_0 + \arctan(\alpha_u/\omega_u) \tag{5}$$

$$|F| = A_0 \exp(-\alpha_u T_0)/\cos(\omega_u T_0 + \Phi_F) \tag{6}$$

Thus, if ω_u and α_u are chosen to obtain realistic peak width and damping, then F can be chosen to fit A_0 and T_0.

Nonlinearity first comes in as we model the OC. The phase space must be at least two-dimensional in order to afford oscillations. Again, restricting the model to the minimal two dimensions z_1, z_2 (in complex notation $z := z_1 + iz_2$) we assume that, by choice of coordinates, z_1 is the observed variable. As discussed in the previous section the experimental results suggest a view of self-generated oscillatory activity rather than passive oscillatory relaxation. Therefore, we map the observed oscillations onto a limit-cycle attractor in the (z_1, z_2)-plane. At the same time the oscillation obviously comes to rest after a sufficiently long time. This resting state is mapped onto a fixed point attractor stable under no-stimulus conditions. In general, bistability of these two attractors is possible. In the presence of noise such bistability allows for stochastic switches from the resting state and vice versa. The observed probabilistic decay of the oscillations will be discussed in terms of such stochastic switching below.

In Fig. 2 we have illustrated the assumptions made about the dynamics of the oscillatory component so far. We sketch the attractor layout as a function of a parameter that measures the strength of an external stimulus. To the left, only the resting state is stable (here illustrated by zero oscillation amplitude $r = 0$). To the right, under sufficiently strong stimulation, the oscillatory state (here illustrated by nonzero oscillation amplitude r) is stable. The two regions may overlap, forming a region of bistability. Points in parameter space where solutions change qualitatively, in particular, lose stability or cease to exist, are called bifurcation points [see, e.g., Guckenheimer and Holmes (1983) for introduction to these ideas]. Near such bifurcation points, local normal form theory provides us with the simplest (in the sense of lowest order in a Taylor expansion) functional form of a dynamical system consistent with the particular bifurcation. This means that any dynamical system with the same local bifurcation behavior can be transformed by a smooth change of coordinates to this normal form. This transformation is valid in a neighborhood of the critical parameter value and locally in phase space close to the bifurcating solutions.

Using the normal form as the functional form of a dynamical model assures structural stability; that means, small deviation of the actual dynamics of a system from the modeled dynamics do not invalidate the bifurcation behavior and, thus, the qualitative properties of the solutions of the dynamics. Moreover, the existence of other solutions in the model, not contained in the bifurcation diagram, is excluded.

In the present case, the two relevant solutions, that is, the fixed point and the limit cycle, may be at a finite distance from each other in parameter and phase space. An approximation to the functional form can be given if we assume, in addition, that the two bifurcations, the instability of the fixed point and the occurrence of the limit cycle, are very close in parameter and phase space. In this case, a codimension-2 normal form can be given for the complete phase diagram. The resulting so-called generalized Hopf normal form reads:

$$\dot{z} = c_z z + \beta z|z|^2 - \gamma z|z|^4 \tag{7}$$

where $\beta, \gamma \in R, \gamma > 0$, and $c_z := \alpha_z + i\omega_z$ are model parameters. These equations become transparent in polar coordinates, $z = r\exp(i\Phi)$, where r is the oscillation amplitude and Φ the oscillation phase, each governed by the following dynamics:

$$\dot{r} = \alpha_z r + \beta r^3 - \gamma r^5 \tag{8}$$

$$\dot{\Phi} = \omega_z \tag{9}$$

The phase equation has the general solution

$$\Phi(t) = \Phi_0 + \omega_z t, \quad \text{with} \quad \Phi_0 = \Phi(t = 0) \tag{10}$$

The amplitude equation (8) can be analyzed with respect to its fixed points given by zeros of its right-hand side. Note that fixed points at nonzero amplitude $\bar{r} > 0$ correspond to limit cycle solutions $z(t) = \bar{r}\exp[i\omega_z t + \Phi_0)]$ of (7). The parameter ω_z can therefore be directly related to the frequency of oscillation observed in experiment.

To assure boundedness of the solutions we fix $\gamma > 0$. The layout of attractors as a function of the two remaining model parameters α_z and β is shown in Fig. 3. Four regions in this parameter plane can be differentiated,

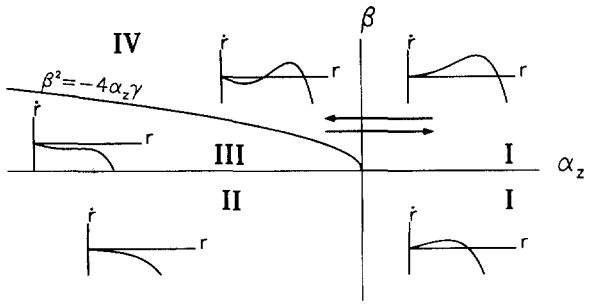

Fig. 3. A phase diagram of (8) in the (α_z, β)-plane shows four regions with qualitatively different phase portraits, here illustrated by plots of the amplitude dynamics: zeros with negative slope indicate stable fixed points, zeros with positive slope unstable fixed points. Fixed points at finite amplitude imply limit cycle oscillation, while fixed points at $r = 0$ imply a stationary state for the complete dynamics. The theoretical picture of the experimental observations is based on assuming that the resting state of the system in the absence of stimulation resides in region IV, the bistable region. A stimulus event is assumed to shift α_z from region IV to region I, as indicated by the *arrows*. This leads to a destabilization of $r = 0$ and thus to a transition to the stable branch at $r \neq 0$, corresponding to the onset of oscillation. After returning to region IV, the system remains trapped in the oscillatory state

based on the existence and stability of fixed points, all of which can be analytically determined in straightforward fashion. The region denoted as region IV contains the phase portrait which expresses our modeling assumptions: a stable fixed point at $r = 0$ coexists with a stable limit cycle at $r = \sqrt{\beta/(2\gamma) + \Delta}$, with $\Delta = \sqrt{[\alpha_z - \beta^2/(4\gamma)]/\gamma}$. The first corresponds to the resting state, the second to the oscillator state. The bifurcation diagram (Fig. 2) summarizing our theoretical assumption is obtained if α_z is considered to be the bifurcation parameter shifted between regions IV and I, as indicated by the arrows in Fig. 3.

3.2 The role of noise

Noise must be included explicitly in the modeling of neuronal time structure not only to account for observable fluctuations present in biological systems, but also for conceptual reasons (cf. Schöner and Kelso 1988). Here stochastic switching among two bistable states of the oscillatory dynamics is mediated by noise, and the noise level affects the time scale of such switches. Based on the typical assumptions (many independent sources of variability with very fast decay of correlations; cf. Horsthemke and Lefever 1984) fluctuations are included in the dynamical model by adding stochastic forces in the form of independent gaussian white noise processes to the dynamic equations. For the oscillatory component, for instance,

$$\dot{z} = c_z z + \beta z|z|^2 - \gamma z|z|^4 + \xi_z(t) \tag{11}$$

where $\xi_z(t) := \xi_1(t) + i\xi_2(t)$ are two independent gaussian white noise processes with $(i, j = 1, 2)$:

$$\langle \xi_i \rangle = 0 \tag{12}$$

$$\langle \xi_i(t)\xi_j(t') \rangle = Q\delta(t - t')\delta_{ij} \tag{13}$$

Here $\langle \cdot \rangle$ denotes the statistical average, and Q measures the noise strength. The transfer component is dealt with analogously.

Variabilities of measured onset times, cycle times, or amplitudes are accounted for in terms of fluctuations described by the stochastic dynamics and depend on both the underlying dynamics and the noise strength. In simulations reported below, the corresponding parameters are chosen so as to reproduce the observed level of fluctuations as well as the observed order of magnitude of mean lifetimes of evoked oscillations ($\approx$400 ms).

Stochastic switching between the resting and the oscillatory state may also account for the observation of spontaneous oscillatory neuronal activity, that is, oscillations observed in the absence of stimulation. The rhythms originating from the thalamocortical system are known to occur spontaneously, and among these the rhythms in the alpha range have been examined in detail with respect to their spontaneous occurrence (Andersen and Andersson 1968; Steriade and Llinás 1988; Steriade et al. 1990). In the experiments referred to here, episodes of variable duration in which spontaneous oscillations with cycle times matching those of the stimulus-evoked oscillations were observed in LFP recordings. An example is shown in panel A of Fig. 5. Such episodes occur as well in the stochastic bistable model as illustrated in the same figure, panel B.

3.3 Coupling the two dynamic components

We have introduced two response components on the basis of their different dynamic properties. Actually, both components are observed through the same neuron. Therefore, the question must be addressed of how the two dynamic components contribute to the one observable time structure of neuronal response. Defining an observable $w(t)$ essentially amounts to defining operationally the nature of the response components $u(t)$ and $z(t)$. The simplest idea is to define the observable time structure $w(t)$ as the superposition of the two dynamic components:

$$w(t) = u(t) + z(t) \tag{14}$$

This means that the components are defined through the limit cases in which the observable time structure contains only a transfer component (as occurs for nonoscillatory cells) or only an oscillatory component (as occurs for spontaneous oscillations). The dynamics of each component defined up to now represent the dynamics in these limit cases.

If both components are observed simultaneously, their interactions must be taken into account. First, with respect to the properties of the transfer component no difference was observed between oscillatory and nonoscillatory cells. Therefore, we assume that the oscillatory component does not couple into the dynamics of the transfer component. Second, the oscillatory component is observed in isolation, that is, without an accompanying transfer response only during spontaneous oscillatory episodes in the absence of stimulation. Fleming and

Evarts (1959) registered evoked oscillatory responses only in conjunction with short-latency (transfer) responses. This suggests that the oscillatory component is coupled to the stimulus only through the transfer component. Another classical observation supports this hypothesis: Chang (1950) reported that the evoked oscillatory time structure is unaffected by a second stimulus if this stimulus fails to elicit a transfer response because it is applied too soon after a first stimulus. To determine the functional form of the coupling of the transfer component into the oscillatory component dynamics we invoke two observations: (1) The evoked oscillations start with a well-defined initial phase observed through the reproducible initial cycle time Z_1. Such an initial phase can be accounted for by the lowest-order additive coupling of u into the oscillatory dynamics, which breaks the rotational symmetry (invariance under phase shift) of the normal form. (2) The presence of a transfer response increases very much the probability of observing oscillations over the case of the absence of a transfer response. Theoretically, this implies that excitation of the transfer component shifts the relative stability of the resting and oscillatory state significantly in favor of the oscillatory state. In the bifurcation diagram (Fig. 2) this means that the transfer response shifts the bifurcation parameter to the right and thus stabilizes the limit cycle while destabilizing the fixed point at $z = 0$. This can be accounted for by multiplicative coupling of u into the oscillatory component.

Based on these assumptions the complete transfer and oscillatory dynamics can be written as

$$\dot{u} = c_u u + FS(t)$$

$$\dot{z} = (c_z + k_1 u)z + \beta z|z|^2 - \gamma z|z|^4 + k_2 u \qquad (15)$$

where k_1 and k_2 are two complex coupling constants. The real part of k_1 affects the stability properties of the oscillatory state, and the imaginary part of k_1 contributes to the frequency of the oscillations in the presence of a transfer response. The phase of k_2 determines the initial phase of the oscillatory response (and hence, Z_1) while its modulus affects the amount of phase shift occurring on secondary stimulation of an ongoing oscillation. Based on these analytical results these coupling parameters can be adjusted to match experimentally observed properties of the neuronal time structure without formal error-minimizing fits.

In Fig. 4 numerical simulation of Eq. (15) illustrates the activation of the different response components and their superposition under the double-stimulus paradigm. The parameter values listed in the figure caption were used for all simulations reported in this paper. The dynamical model captures the essential experimental effects: (1) spontaneous oscillatory episodes, (2) probabilistic duration of episodes under OPS conditions, and (3) the modulation of the oscillatory time structure depending on the phase at which a second stimulus is applied during an ongoing oscillation. A comparison of properties 1 and 3 between experimental and simulated data is given in Fig. 5.

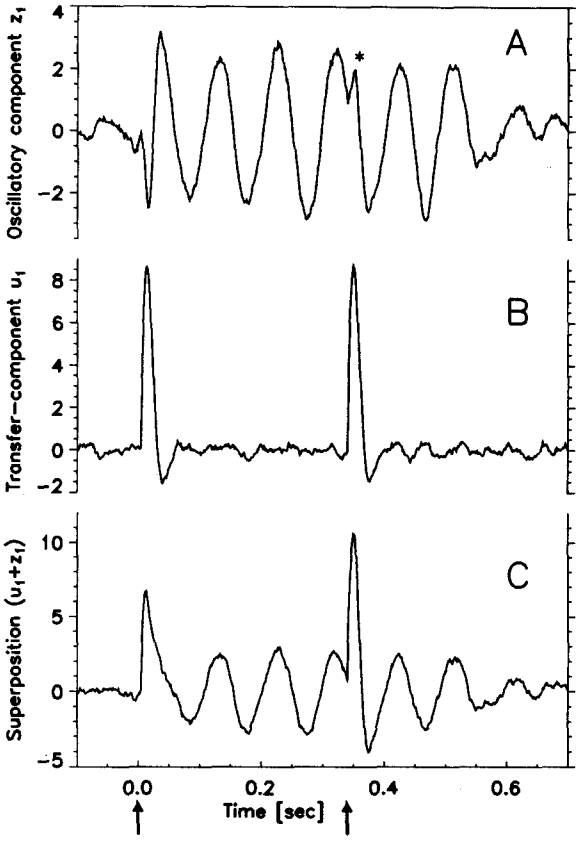

Fig. 4A–C. Activity of response components in a simulated double-stimulus paradigm. The first stimulus is given at $t = 0$ and the second after a delay of 340 ms, as indicated by the *arrows*. **A** The oscillatory component is activated at $t = 0$, and the second stimulus induces only weak effects on the phase and amplitude of the oscillation at this particular value of interstimulus interval (ISI), even though the oscillation was started at $t = 0$ by identical stimulation (cf. data in Fig. 1). The small peak indicated by the asterisk is the only visible influence. After about 550 ms the oscillation decays spontaneously. **B** Transient, stereotype activation of the transfer component by both stimuli. **C** Superposition of **A** and **B**, which models the observable signal. The parameters are chosen in such a way that (1) oscillations can be evoked reliably by stimulation, (2) the frequency of oscillation is 10 Hz, (3) the first cycle time is greater than the following ones, (4) the average length of evoked oscillatory episodes is about 400 ms, (5) latency peaks are sharper by an approximate factor of 5 than oscillatory peaks, as observed in experiment. Parameters used: $\alpha_z = -23$ Hz; $\beta = 10$ Hz: $\gamma = 1$ Hz; $\omega_z = 2\pi \times 10$ Hz; $\alpha_u = -60$ Hz; $\omega_u = 115$ Hz; $k_1 = -12i$ Hz; $k_2 = 12$ Hz; $F = -17i$. All noise levels are set to $Q = 4$ Hz. These parameters are held fixed in all simulations shown throughout this article, unless stated otherwise

3.4 Oscillation lifetimes

The lifetimes of oscillatory response patterns can be used as a window into the underlying system dynamics. Empirically, the lifetime of the oscillatory state can be estimated by determining the time T_L at which the last detectable peak is observed. For 9 of 11 oscillatory cells T_L was determined on the basis of PSTHs for all ISI conditions. (The two excluded cells had clear indications of nonstationary during the 1-h measurement time for a complete ISI scan.) The mean lifetime under OPS

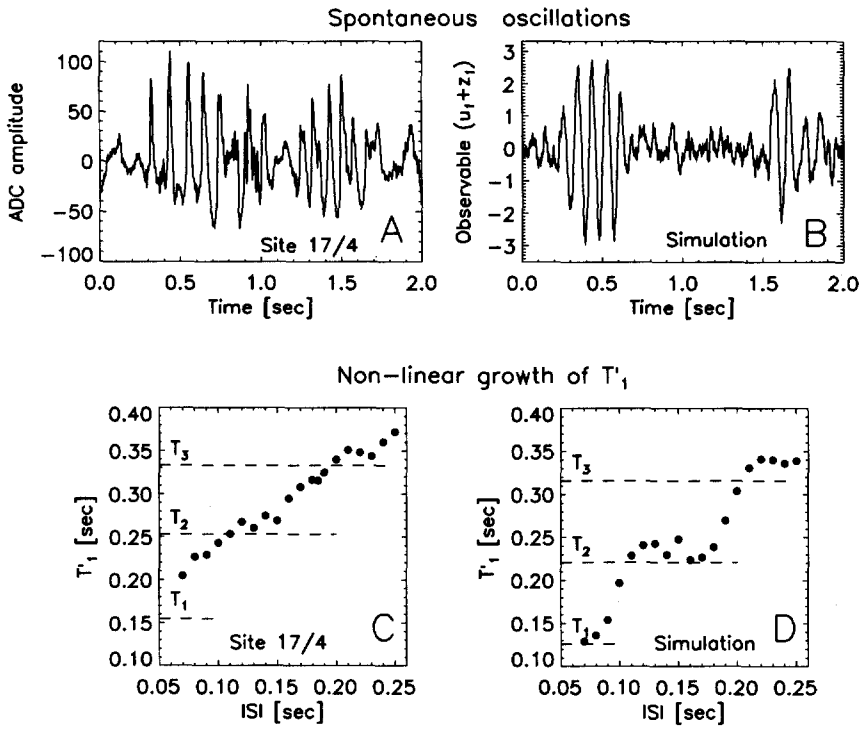

Fig. 5A–D. Comparison of model features with recorded data. **A** Spontaneous oscillatory episodes in a local field potential (LFP) recording. Two pronounced oscillation "spindles" do appear. **B** Same phenomenon in a simulated run. The noise intensity is increased ($Q = 9$ Hz), compared with that of Fig. 4, to increase the probability of spontaneous oscillatory events. **C** The time of first oscillatory peak after the second stimulus, extracted from PSTH data, is plotted against ISI. There are two obvious plateaus in the vicinity of the times where peaks from the response to the first stimulus would be expected (indicated by T_2, T_3). Over the range of a plateau, the oscillations elicited by the first stimulus are unaffected in timing by the second one. **D** Same diagram as panel **C** for simulated data. Each point is extracted from an average signal of eight identical runs. Plateaus are more pronounced than in **C**. Note that parameters were not chosen to fit these plateaus, but according to the points listed in the caption of Fig. 4

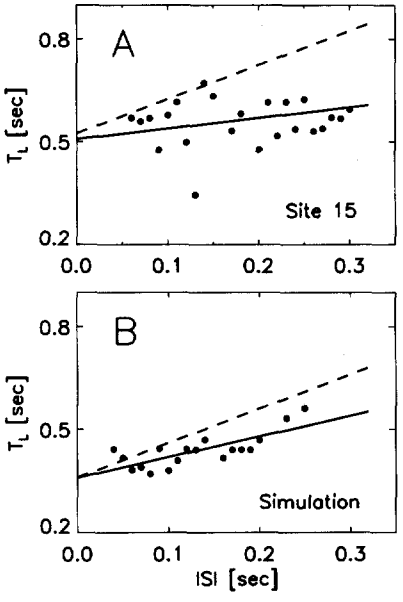

Fig. 6. **A** Typical example of the dependence of the time of last oscillatory peak T_L on ISI in a double-stimulus paradigm. *Filled dots* correspond to measured points extracted from PSTHs; the *continuous line* is found by linear regression (slope is 0.3 in this example), and the *dashed line* starts from the mean lifetime derived from oscillations per se (OPS) conditions and increases with slope 1. This increase would be expected if the oscillatory response after the second stimulus would be a restarted version of the first response. **B** Same plot as in **A** but obtained from simulations mimicking the experimental double-stimulus paradigm

conditions across the 9 cells was found to be $\bar{T}_{ops} = 526$ ms. Panel A in Fig. 6 shows T_L for a typical cell as a function of ISI jointly with a linear regression of this relationship. The resulting slope of the regression curve can be contrasted to the hypothetical case where the second stimulus in the double-stimulation paradigm starts a new, independent oscillation each time. Then the lifetime measured from the second stimulus should be independent of ISI and equal to the mean lifetime under OPS conditions. As measured from the first stimulus, T_L should increase linearly with slope 1 from the mean lifetime under OPS conditions as indicated by the dashed lines in Fig. 6. The observation that the measured lifetimes lie below this limit (statistically the mean regression slope of $\bar{b} = 0.4 \pm 0.1$ is significantly different from both 0 and 1) indicates that the oscillations following the second stimulus are affected by that stimulus but carry information from their own past.

The dynamical model reproduces this experimental finding. A series of simulations exactly mimicking the experimental paradigm was analyzed in the same fashion as the experimental data. The result shown in panel B of Fig. 6 matches the experimental observation.

It is possible to pinpoint more precisely which aspect of the theory accounts for the particular ISI dependence of lifetimes. The following discussion abstracts from the details of the dynamical model and aims to show that bistability as a concept provides a quantitative explanation of the lifetime statistics. We consider an abstract bistable dynamical system in the presence of fluctuations with the two stable states, R (for resting state) and O (for oscillatory state). We make three assumptions: (1) R is more stable than O so that stochastic switches from R to O are very unlikely; (2) a switch from R to O is induced with probability 1 by an external stimulus; (3) applying a stimulus within state O does not affect the system. We are interested in the stochastic switching process from

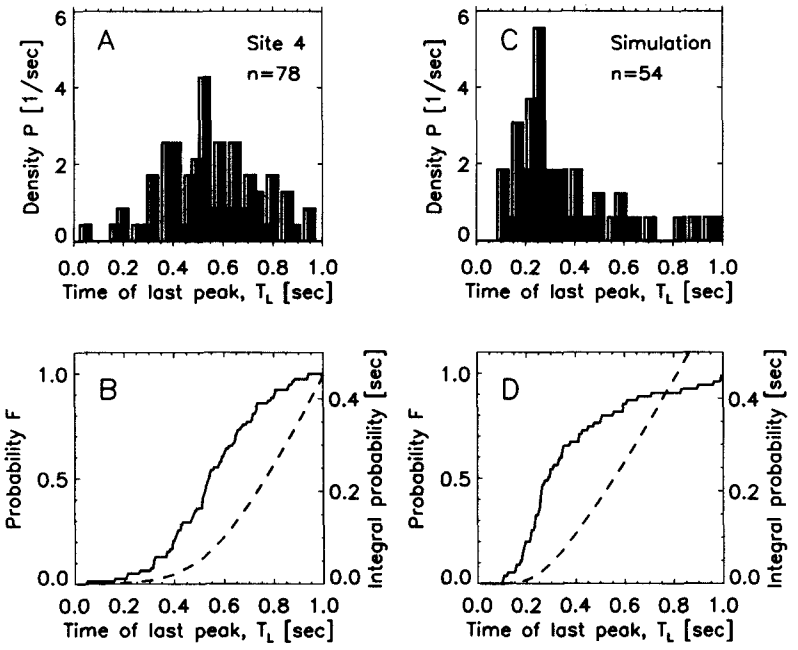

Fig. 7. **A** Estimation of the probability density P for a multiunit recording, obtained from a histogram with a binsize of 30 ms, of 78 measurements of the time of last peak under OPS conditions. The histogram is normalized to give a total area of 1 to allow the interpretation as a probability density. The mean of this distribution is 540 ms. **B** Estimation of functions needed to predict the ISI-dependent lifetime in the double-stimulus paradigm. *Continuous line* and *left scale*: probability F derived from the same data as **A** by integration (cumulative histogram). *Dashed line* and *right scale*: the integral probability derived from F by further integration. **C, D** Results of an equivalent analysis of a simulated data set. The mean lifetime was 364 ms for this sample and parameters listed in Fig. 4

stochastic dynamical systems provides us with the concept of first passage time τ (cf. Gardiner 1983). The first passage time from O to R is a random variable, and its probability density $P(\tau)$ is well defined. For purposes of calculation, the distribution function $F(T)$ defined as

$$F(T) = \int_0^T P(\tau)\mathrm{d}\tau \tag{16}$$

is useful. $F(T)$ is the probability that a switch from O to R occurs in the time interval $[0, T]$.

To relate these concepts to experimental measures, consider first OPS data. The times T_L at which the last discernible peak occurs in unaveraged data samples the probability density $P(\tau)$. We have performed the same analysis as for PSTH data for three sets of data (two single-unit recordings, one multiunit recording) for which responses were sufficiently vigorous to estimate T_L from unaveraged spike data. These estimates were extracted from smoothed spike trains obtained by convolving the raw spike trains with a gaussian of 10 ms width (cf. MacPherson and Aldridge 1979). Note that the gaussian filter induces no phase shifts. Figure 7A and B shows a sampling of $P(\tau)$ and $F(T)$ obtained from one of the three recordings. A total of about 80 independent measurements of T_L in individual trials at appropriate OPS conditions (ISI = 2000, 1000, and 800 ms) were obtained to calculate the histogram. The mean of this distribution, $\bar{T}_{ops}$, is an estimate of the mean first passage time. The cumulative histogram samples the distribution function, $F(T)$ as shown in part B of the figure. Panels C and D show the result of the analysis of a simulated data set.

Based on these estimates from the OPS data it is possible to predict the ISI dependence of $\bar{T}_L$ in the double-stimulus paradigm[2]. For simplicity of notation, ISI is denoted as I in the formulas below. Consider the random variable τ, defined as the time in the double-stimulus paradigm when the switch from O to R occurs after the second stimulus. Its probability density $Q(I, \tau)$ depends on ISI. There are two contributions to this probability density. First, in cases in which the switch has already occurred before the second stimulus, that stimulus puts the system back into state O with probability 1 and the decay probability counting from ISI must be calculated (cf. assumption 2 of the definition of the idealized system above). Second, in cases, where the system has not decayed before the second stimulus is applied, that stimulus does not, in our abstract bistability model, affect the lifetime of O (assumption 3 above), and we must obtain the probability density of the OPS case. The mathematical derivation given in the Appendix leads to the following formula:

$$Q(I, \tau) = F(I)P(\tau - I) + P(\tau) \tag{17}$$

For large I, $Q(I, \tau)$ is dominated by the first term of this equation because the transition $O \rightarrow R$ has occurred with high probability before the second stimulus. In this limit case, $F(I) \approx 1$, and $P(\tau) \approx 0$ for $\tau > I$ so that the probability Q reduces to a time-shifted OPS distribution P.

The mean first passage time in the DSP at a fixed I can now be calculated as

$$\bar{T}_L(I) := \int_I^\infty \tau Q(I, \tau)\mathrm{d}\tau \tag{18}$$

[2] Estimates of the mean lifetime are less sensitive to noise than estimates of the distribution of lifetimes, because the mean value is an integral measure compared with the probability distribution. Therefore, we did not compare theoretical and estimated distributions

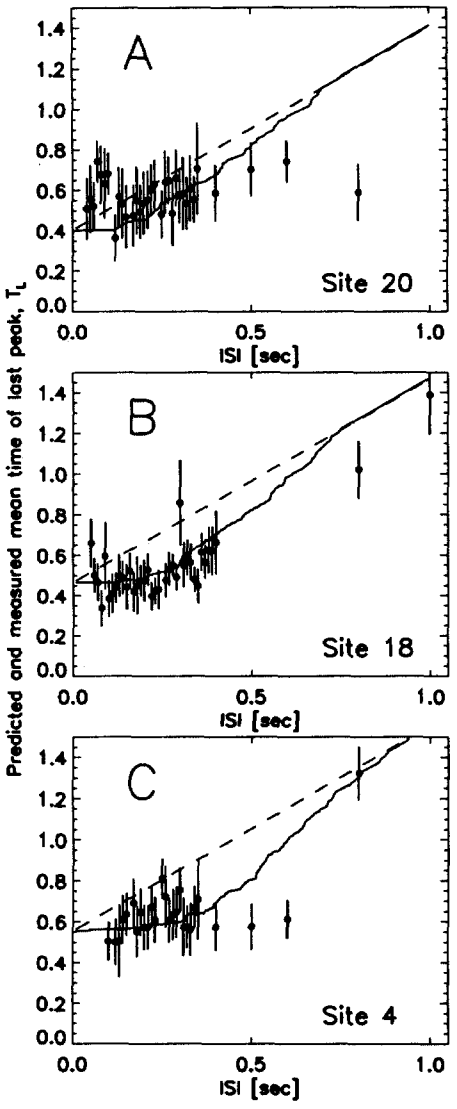

Fig. 8A–C. Predicted and measured mean lifetime of oscillations as a function of ISI in the double-stimulus paradigm for three recordings. **A, B** Single units; **C** multi unit. Each *filled dot* is the average of about 30 measurements from unaveraged data, with the corresponding standard deviations indicated as error bars. All three plots include totally about 3000 independent measurements of T_L.The *continuous lines* correspond to the prediction calculated with (19).The *dashed lines* start from the mean lifetime derived from OPS conditions and increase with slope 1, representing the case of a pure restart (cf. Fig. 6)

and this is the quantity which corresponds to estimates of the mean T_L for a given interstimulus interval I. Inserting (17) and performing some mathematical transformation we find a formula for $\bar{T}_L(I)$ that depends only on $F(T)$ and the mean first passage time in the OPS case, $\bar{T}_{ops}$ (see Appendix for derivation):

$$\bar{T}_L(I) = [1 + F(I)]\bar{T}_{ops} + \int_0^I F(T)\mathrm{d}T \qquad (19)$$

Given the OPS estimates of F and $\bar{T}_{ops}$ (cf. Fig. 7), the ISI dependence of $\bar{T}_L$ can be predicted without any further free parameters. Figure 8 shows the predicted curves

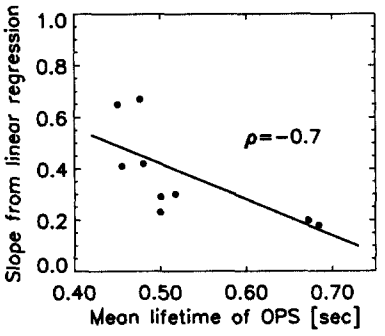

Fig. 9. Correlation of mean lifetimes of the OPS with the slopes derived from a linear regression of the ISI dependence of mean lifetime in the double-stimulus paradigm (cf. Fig. 6). The coefficient of correlation is $\rho = -0.7$, which is in good agreement with the predicted anti-correlation described in the text

jointly with the corresponding experimental estimates. The agreement is excellent in view of the variability of the experimental estimates.

A further check can be based on the following thought. The slope of $\bar{T}_L(I)$ must be less than 1 because this is the slope of the hypothetical limit case of a restart. The deviation of $\bar{T}_L(I)$ from the slope 1 curve is indicative of the contribution of those probability events in which the oscillations "go through" the second stimulus. Therefore, we expect the slope to be closer to 0 for vigorously oscillating cells with long lifetimes and closer to 1 for badly oscillating cells with short lifetimes of the oscillatory state. This prediction can be tested by correlating the slopes of the $\bar{T}_L(I)$ regression obtained from averaged data with the mean lifetime under OPS conditions. In the experiments this correlation is found to be negative ($\rho = -0.7$, significant with 4% error) as predicted (see Fig. 9).

4 Discussion

Experiments probed the dependence of the temporal structure of evoked oscillatory responses of cortical neurons on the temporal structure of peripheral stimuli. Theory for this observed dependence was based on the assumption that at the observable level dynamic laws can be identified. Variables were chosen to account for different dynamic components of the neuronal response, the transfer, and the oscillatory component. A dynamical model was based on the phase diagram reconstructed from the experimental data, which included a bistable region with an oscillatory and a resting state. The dynamic model was compared with the experimental results. Abstracting from the functional form of the model it was shown how the dependence of lifetime on the interstimulus interval can be derived from the principle of bistability of oscillatory and resting state.

What is certainly unusual and possibly unfamiliar about the theoretical approach reported here is that a quantitative account of cortical response behavior is attempted without reducing the description to biophysical

models of neurons and their circuits. We argue that the approach expounded here in the context of a concrete example is relevant because (1) it fosters a close link of theory and experiment, (2) it is capable of discovering principles underlying the temporal organization of neuronal response, and (3) it provides constraints for reductionistic neuronal modeling. The first point is illustrated by the interrelation between dynamic model and experimental paradigm: asking the theoretical question for the nature of the coupling of neuronal response to stimulation led to the experimental paradigm of double stimulation. On the other hand, that paradigm, commonly used also in other contexts, gains a new significance in light of the dynamic interpretation. Consider, as a second illustration, the methods of analysis developed here. Asking, for instance, the theoretical question of how in a bistable system the decay of the oscillatory state can be understood, the measure T_L of oscillation lifetime was developed, and in terms of this measure the experimental data revealed additional, hitherto overlooked structure. In relation to the second point, the linkage of the principle of bistability to the statistics of lifetime may serve as an illustration. Note that the theoretical method is, in principle, a general one.

To address the third point of how dynamic models constrain reductionistic models we discuss first the possible structural underpinnings of the effects reported in this paper. Clearly, the dynamics of the transfer component involve structurally the entire afferent path from mechanoreceptors to the primary somatosensory cortex. Synaptic interactions of all neurons along this path contribute to the observed latencies and response amplitudes. Thus far, even the standard system theoretical picture used for the transfer component represents "collective" dynamics, that is, the effective dynamics of a set of tightly interrelated neurons. The structural support of the oscillatory component is less clear, although extensive experimental and modeling work exists on cortical and thalamic sources of oscillations in the 10-Hz range [for recent reviews see Steriade and Llinás (1988) and Connors and Gutnick (1990)]. Based on this work the most likely picture is one in which groups of neurons are involved in generating 10-Hz rhythms in vivo. Individual neurons, in particular nuclei of thalamus, are capable of generating such rhythms in vitro, but the observation of highly synchronized mass signals in vivo suggest that the interaction among cells is important for the oscillatory response component of neurons in intact structures as studied here. Hence, the oscillatory dynamics is structurally almost certainly again a "collective" one.

Attempts to model the generation of temporal structure from models of such underlying neuronal circuitry face a number of problems of which we single out two. First, the properties of individual components – for example, various kernels of thalamus or various types of cells – may be different when studied in isolation than when studied in the intact system. Second, the solutions of such structural models depend often qualitatively on structural parameters such as synaptic efficacy and synaptic transmission delay. These parameters are, however, not easily measurable, and, more importantly, not manipulable! As a result, mechanisms underlying the generation of observed patterns of excitation remain speculative. With respect to both of these problems the theoretical approach espoused here can serve to constrain reductionistic models. The collective variables and dynamics may indicate which properties of the individual components and of their interaction is relevant with respect to the macroscopic temporal structure to be explained. Furthermore, from a reductionistic model it may be easier and more systematic to derive a macroscopic dynamics rather than to derive directly the macroscopic solutions. For instance, it may be significant and possible to show that a reductionistic model affords bistability of oscillatory and resting state for a range of structural parameters. Finally, the theoretical methods could be employed to investigate how far the dynamic properties of temporal structure observed at the macroscopic level of EEG and evoked potentials (Basar et al. 1992) match the dynamic properties of oscillations at the cellular level.

The finding that oscillatory and resting state may coexist bistably is potentially of wider significance than suggested by the phenomenon under study here. First, this finding shows very clearly that temporal structure can be actively self-generated by neuronal structures. This may be an important message to consider when the stimulus dependence of temporal response structure is studied, as done, for instance, by Richmond et al. (1990) in visual and infratemporal cortex. Second, the dynamical account of oscillations coexisting with transfer response components may be useful to understand similar phenomena in other structures of the nervous system such as evoked oscillations in the olivocerebellar system (Llinás and Sasaki 1989) discussed in the context of coordination of movement, or in the temporal pole of awake monkeys (Nakamura et al. 1991) in the context of recognition and short-term memory. In this latter case, the persistence of stimulus-related, temporal structure in the face of peripheral and internal influences might support a function of keeping information available on a time scale of hundreds of milliseconds. Bistable processes have also been reported at the single-cell level (Silva et al. 1991).

Acknowledgements. We thank Sabine Kopecz for help with the analysis tools and for drawing our attention to effects in lifetime. This work was supported through grants from the Deutsche Forschungsgemeinschaft, Bonn, the Ministerium für Wissenschaft und Forschung, Düsseldorf and the Bundesministerium für Forschung und Technologie, Bonn.

Appendix
Mean first-passage time in stochastic bistable dynamics for the double-stimulus paradigm

Let D_{t_1,t_2} denote the event "the stochastic switch from O to R occurs in the time interval $[t_1, t_2]$". The probability of this event under OPS conditions is by definition

$$Prob_{ops}(D_{t_1,t_2}) = F(t_2) - F(t_1) \tag{20}$$

To calculate a corresponding probability for the double-stimulus paradigm observe first

$$Prob_{dsp}(D_{I,\tau}) = Prob_{dsp}(D_{0,I} \text{ and } D_{I,\tau}) + Prob_{dsp}(\overline{D_{0,I}} \text{ and } D_{I,\tau}) \quad (21)$$

where $\overline{D_{0,I}}$ is the event that no decay occurs within the indicated time interval. The first term is transformed by invoking conditional probability as follows:

$$\begin{aligned} Prob_{dsp}(D_{0,I} \text{ and } D_{I,\tau}) &= Prob_{dsp}(D_{0,I}) Prob_{dsp}(D_{I,\tau} | D_{0,I}) \\ &= Prob_{ops}(D_{0,I}) Prob_{ops}(D_{0,\tau-I}) \\ &= F(I)F(\tau - I) \end{aligned} \quad (22)$$

where we have used the assumption that the stimulus at I puts the system with probability 1 into the O state (see main text). Invoking the assumption that further stimulation does not affect the system if it is already in the oscillatory state, the second term in (21) can be rewritten as

$$\begin{aligned} Prob_{dsp}(\overline{D_{0,I}} \text{ and } D_{I,\tau}) &= Prob_{ops}(D_{I,\tau}) \\ &= F(\tau) - F(I) \end{aligned} \quad (23)$$

Adding the two terms and differentiating with respect to τ yields the probability density

$$Q(I,\tau) = F(I)P(\tau - I) + P(\tau) \quad (24)$$

defined in the main text. This function is correctly normalized:

$$\int_I^\infty Q(I,\tau)\mathrm{d}\tau = 1 \quad (25)$$

as a little calculation shows. Inserting $Q(I,\tau)$ into (18) we obtain:

$$\begin{aligned} \bar{T}_L(I) &= \int_I^\infty \tau P(\tau)\mathrm{d}\tau + F(I)\int_I^\infty \tau P(\tau - I)\mathrm{d}\tau \\ &= \int_I^\infty \tau P(\tau)\mathrm{d}\tau + F(I)\int_0^\infty (t + I)P(t)\mathrm{d}t \\ &= \int_I^\infty \tau P(\tau)\mathrm{d}\tau + F(I)(\bar{T}_{ops} + I), \text{ with} \end{aligned}$$

$$\bar{T}_{ops} := \int_0^\infty tP(t)\mathrm{d}t$$

where $\bar{T}_{ops}$ is the mean lifetime in the single-stimulus paradigm. The first term can be conveniently expressed as

$$\int_I^\infty \tau P(\tau)\mathrm{d}\tau = \bar{T}_{ops} - G(I), \quad \text{with } G(I) := \int_0^I \tau P(\tau)\mathrm{d}\tau$$

so that

$$\bar{T}_L(I) = [1 + F(I)]\bar{T}_{ops} + IF(I) - G(I)$$

Integrating by parts

$$G(I) = IF(I) - \int_0^I F(T)\mathrm{d}T \quad (26)$$

we finally obtain

$$\bar{T}_L(I) = [1 + F(I)]\bar{T}_{ops} + \int_0^I F(T)\mathrm{d}T \quad (27)$$

References

Adrian ED (1941) Afferent discharges to the cerebral cortex from peripheral sense organs. J Physiol (Lond) 100:159–191

Aitkin LM, Dunlop CW, Webster WR (1966) Click-evoked response patterns of single units in the medial geniculate body of the cat. J Neurophysiol 29:109–123

Andersen P, Andersson SA (1968) Physiological basis of the alpha rhythm. Appleton-Century-Crofts, New York

Basar E (ed) (1980) EEG-brain dynamics. Relation between EEG and brain evoked potentials. Elsevier/North-Holland, Amsterdam

Basar E, Basar-Eroglu C, Parnefjord R, Rahn E, Schürmann M (1992) Evoked potentials: ensembles of brain induced rhythmicities in the alpha, theta and gamma ranges. In: Basar E, Bullock TH (eds) Induced rhythms in the brain. Birkhäuser, Berlin, pp 155–181

Bishop GH, O'Leary J (1936) Components of the electric response to the optic cortex of the rabbit. Am J Physiol 117:292–308

Chang H-T (1950) The repetitive discharges of cortico-thalamic reverberating circuit. J Neurophysiol 13:235–257

Connors BW, Gutnick MJ (1990) Intrinsic firing patterns of diverse necortical neurons. Trends Neurosci 13:99–104

Dinse HR, Krüger K, Best J (1990) A temporal structure of cortical information processing. Concepts Neurosci 1:199–238

Fleming TC, Evarts EV (1959) Multiple response to photic stimulation in cats. Am J Physiol 197:1233–1236

Ganz L, Felder R (1984) Mechanism of directional selectivity in simple neurons of the cat's visual cortex analyzed with stationary flash sequences. J Neurophysiol 51:294–324

Gardiner CW (1983) Handbook of stochastic methods. Springer, Berlin Heidelberg New York, pp 132–142

Guckenheimer J, Holmes P (1983) Nonlinear oscillations, dynamical systems, and bifurcations of vector fields. Springer, Berlin Heidelberg New York, pp 358–360

Horsthemke W, Lefever R (1984) Noise-induced transitions. Springer, Berlin Heidelberg New York

Llinás R, Sasaki K (1989) The functional organization of the olivo-cerebellar system as examined by multiple purkinje cell recordings. Eur J Neurosci 1:587–602

MacPherson JM, Aldridge JW (1979) A quantitative method of computer analysis of spike train data collected from behaving animals. Brain Res 175:183–187

Movshon JA, Thompson ID, Tolhurst DJ (1978) Receptive field organization of complex cells in the cat's striate cortex. J Physiol (Lond) 283:79–99

Nakamura K, Mikami A, Kubota K (1991) Unique oscillatory activity related to visual processing in the temporal pole of monkeys. Neurosci Res 12:293–299

Richmond BJ, Optican LM, Spitzer H (1990) Temporal encoding of two-dimensional patterns by single units in primate primary visual cortex. I. Stimulus-response relations. J Neurophysiol 64:351–369

Schöner G, Kelso JAS (1988) Dynamic patterns generation in behavioral and neural systems. Science 239:1513–1520

Schöner G, Kopecz K, Spengler F, Dinse HR (1992) Evoked oscillatory cortical responses are dynamically coupled to peripheral stimuli. NeuroReport 3:579–582

Silva LR, Amitai Y, Connors BW (1991) Intrinsic oscillations of neocortex generated by layer 5 pyramidal neurons. Science 251:432–435

Steriade M, Llinás RR (1988) The functional state of the thalamus and the associated neuronal interplay. Physiol Rev 68:649–742

Steriade M, Gloor P, Llinás RR, Lopes da Silva FH, Mesulam M-M (1990) Basic mechanisms of cerebral rhythmic activities. Electroencephalogr Clin Neurophysiol 76:481–508